Protonolysis of the Hg−C Bond of Chloromethylmercury and Dimethylmercury. A DFT and QTAIM Study

Boris Ni,[†,‡] James R. Kramer,[‡] Russell A. Bell,[†] and Nick H. Werstiuk*[,†]

Department of Chemistry and School of Geography and Earth Science, McMaster University, Hamilton, Ontario L8S 4M1, Canada

Received: March 24, 2006; In Final Form: June 8, 2006

Possible mechanisms for degrading chloromethylmercury (CH_3HgCl) and dimethylmercury [$(CH_3)_2Hg$] involving thiol and ammonium residues were investigated by DFT and atoms-in-molecules (QTAIM) calculations. Using H_2S and HS^- as models for thiol and thiolate groups RSH and RS^-, respectively, we obtained transition states and energy barriers for possible decomposition routes to $Hg(SH)_2$ based on a model proposed by Moore and Pitts (Moore, M. J.; Distefano, M. D.; Zydowsky, L. D.; Cummings, R. T.; Walsh, C. T. *Acc. Chem. Res.* 1990, *23*, 301. Pitts, K. E.; Summers, A. O. *Biochemistry* **2002**, *41*, 10287). Demethylation was found to be a multistep process that involved initial substitution of Cl^- by RS^-. We found that successive coordination of Hg with thiolates leads to increased negative charge on the methyl group and facilitates the protonolysis of the Hg−C bond by H−SH. This was also found to be the case for $(CH_3)_2Hg$. We found that NH_4^+ readily protonolyzes the Hg−C bond of these thiolate complexes, suggesting that ammonium residues of protonated amino acids might also act as effective proton donors.

Introduction

Mercury compounds are important pollutants in the environment and are the more toxic metal compounds accumulated and retained by living organisms.[1−6] $MeHg^+$ usually exists as CH_3HgCl (CMM) and CH_3HgOH[6] in oxic waters.[2] Much effort has been devoted to the investigation of the degradation of mercurial compounds because of concerns about toxicity and bioaccumulation. The total concentration of MeHg in fish often is near and sometimes exceeds the level of 0.5−1 μm considered to be safe for human consumption.[2,4,6] Two main processes for the conversion of organomercurials into less toxic species have been proposed: photoreduction and microbial-assisted transformations.[2,7−9]

Degradation of MeHg under UV and sunlight radiation in lakes and seawater has been studied experimentally and theoretically.[10−14] Tossell[14] demonstrated that dissociation of $(Me)_2Hg$ occurs through excited states with energies in the range ~4.4 eV. He showed that the lowest triplet state of CH_3HgCl is dissociative, leading to decomposition into CH_3 and HgCl radicals. Another possible mechanism of MeHg photodecomposition was proposed by Chen et al.,[15] who suggested that the Hg−C bond is attacked by the electronically excited OH radical that is produced during photolysis.

Biotic reduction of Hg(II) into Hg(0) can occur through bacterial enzymatic catalysis.[9,16−21] In particular, two enzymes, MerA and MerB, are responsible for efficient detoxification of both ionic and organomercurial compounds. The organomercurial lyase MerB catalyzes protonolysis of the Hg−C bond, resulting in Hg(II), which is reduced to less toxic Hg(0) by reductase MerA.[18,19] According to the model proposed by Moore et al.[19] and developed by Pitts and Summers,[20] sulfur-containing amino acid residues of MerB, such as cysteine, could form a complex with an organomercurial material. NMR spectroscopic studies on MerB by Di Lello et al.[22] confirmed previous suggestions that several residues, namely, Cys^{96}, Cys^{159}, and Cys^{160} are critical in determining the activity of MerB. NMR chemical shifts provided evidence that at least two cysteines, Cys^{96} and Cys^{159}, are bound to mercury.[22] This complexation possibly activates the carbon−mercury bond for protonolysis.

Although there is no detailed established reaction mechanism for the protonolysis of the CH_3−Hg bond, there is considerable stereochemical[18,19] and chemical evidence to strongly suggest an overall mechanistic pathway for demethylation. However, possible intermediates and energy barriers involved in the transformations are unknown. The specific impact of the complexation of thiol or amino groups is still uncertain. Protonated amines that are ubiquitous in proteins must also be considered as potential proton donors. In this regard, the reported order of binding to ligands in organic matter is thiol ($\log K = 16-22$) > amine ($\log K = 7.4-8.8$) > carboxyl ($\log K = 1.1-3.5$).[28]

Cleavage of the Hg−C bond of several sulfomercurial compounds $[MeHg([9])aneS_3]^+(BF_4)^-$ was recently studied experimentally and theoretically.[21] The barrier for proton transfer from fluoromethanesulfonic acid (CF_3SO_3H) was found to be substantially lower in three-coordinate $[MeHg(MeSCH_2CH_2SMe)]^+$ and four-coordinate $[MeHg([9])aneS_3]^+$ than in two-coordinate MeHgCl. However, the reaction occurs in a strongly acidic medium and is not expected to be important under biotic conditions. The barrier for protonolysis of MeHgSMe by methanethiol that might be analogous to an enzymatic mechanism was determined to be too high (39 kcal mol^{-1}) to be considered as a realistic pathway for the Hg−C bond-breaking reaction. A computational study on the protonolysis of MeHg by haloacids was recently performed by Barone et al.[23−25] They found that the barriers are strongly influenced by the electronegativity of the ligands and decrease by ~50% upon going from CH_3HgCl to CH_3HgCH_3.

The goal of our study was to evaluate the use of molecular calculations to better understand the demethylation process and

* Corresponding author. E-mail: werstiuk@mcmaster.ca.
† Department of Chemistry.
‡ School of Geography and Earth Science.

10.1021/jp061852+ CCC: $33.50
Published on Web 07/13/2006

to gain fundamental information on possible mechanisms for the action of MerB. Our plan was to explore, computationally, possible routes for degrading CMM and DMM (Dimethylmercury) to $Hg(SH)_2$, a key step being the protonolysis of the Hg−C bond. We focused our study on the proposals made on the basis of recent experimental studies.[19,20,22] We obtained intermediates and energy barriers for their reactions and used QTAIM calculations to analyze the bonding.[26,27] We examined the dependence of the protonolysis barrier on the coordination of the mercury atom as proposed by Wilhelm et al.[21] In addition to thiolates, lysine and other ammonium groups are common in proteins. Therefore, we also explored the possibility of protonolysis of CH_3HgCl by ammonium groups. We present and discuss the results of this work herein.

Computational Methods

DFT calculations were carried out with Gaussian 98 and Gaussian 03[29] at the Becke3PW91 level.[30] Barone et al.[25] employed DFT(LDA) and MP2 methods in an investigation of Hg−C bond cleavage in mercury halides and demonstrated that the accuracy of DFT predictions was comparable with that of the more resource-demanding MP2 method. The 6-311+G(d) basis set was used in geometry optimizations for all elements except Hg, for which we used the ECP60MWB[31] basis set that incorporates the Wood−Boring quasirelativistic effective core potential (ECP). We chose this basis set for Hg because it has been used successfully by Wilhelm et al.[21] and Cox[32] to reproduce experimental geometrical parameters and NMR shifts. The maximum deviation in the calculated and measured Hg−C and Hg−S bond distances of $[MeHg([9])aneS_3)]^+$ does not exceed 0.16 Å.[21] Also, experimentally measured NMR shifts for the carbon of CH_2 of a thioether ligand were accurately reproduced by computation.[21] Vibration analyses were performed for all complexes and transition structures in order to obtain zero-point energies and confirm transition states. The Cartesian coordinates of the optimized geometries and transition states are included in the Supporting Information.

Because QTAIM analyses[26,27] require wave functions obtained with all-electron basis sets, we carried out single-point calculations with all-electron basis sets on optimized geometries obtained at the Becke3PW91/ECP60MWB level. In addition to using the 6-311+G(d) basis set for second- and third-row elements, we employed the relativistic all-electron basis set contracted as [14s11p5d2f].[33] It has been shown to predict the excitation energies and the ionization potential of the Hg atom with an accuracy of better than 2.6%. Relativistic effects, which must be included for heavy elements such as Hg, were treated by employing the Douglas−Kroll−Hess (DKH) Hamiltonian implemented in Gaussian 03. Optimization of a molecular geometry at the B3PW91/ECP60MWB level was followed by a single-point relativistic calculation. This approach is justified because DKH analytical gradients are computationally demanding to evaluate and relativistic corrections to core orbitals are only weakly dependent on geometry.[34] QTAIM analyses were carried out with AIM2000.[27] Molecular structures obtained with AIM2000 are displayed in Figures 1−4.

Results and Discussion

Reaction of Chloromethylmercury (CMM) and Substitution Products. The mechanistic model proposed by Moore et al.[19] and developed by Pitts and Summers[20] is based on coordination of organomercurials with one or two thiolate groups of cysteine residues. The high affinity of mercurials toward thiolates is well-known.[2,35,36] Consequently, we first focused on the complexation of CMM with thiols and thiolates to establish how the barrier for the protonolysis of the Hg−C bond depends on mercury coordination. We approximated the cysteine residue with H_2S and SH^- in our calculations. H_2S and SH^- are considered valid surrogates for cysteine because of the strong Hg−S covalent bond and assumed lesser influence of adjacent atoms. We searched for complexes of CMM and DMM with one or more H_2S and HS^- groups and transition states for possible protonolysis reactions.

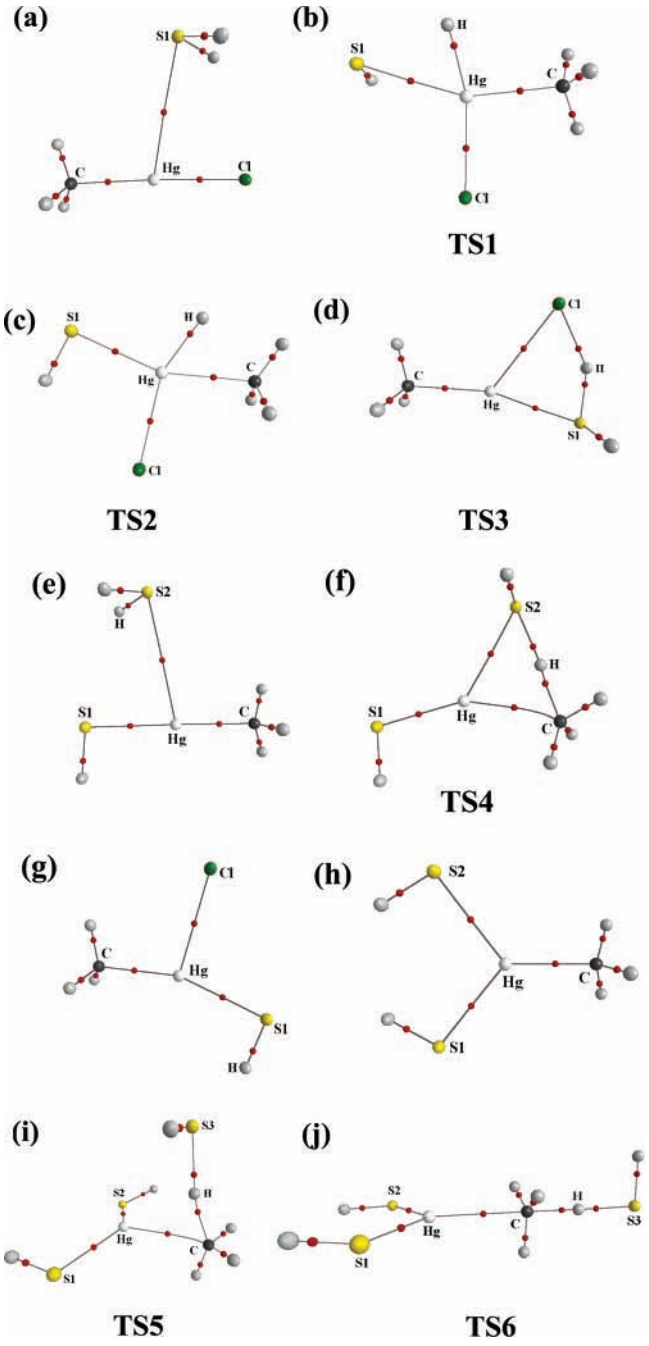

Figure 1. Calculated molecular structures of (a) $[CH_3HgClH_2S]$, (b) **TS1**, (c) **TS2**, (d) **TS3**, (e) $[CH_3HgSH_2S]$, (f) **TS4**, (g) $[CH_3HgClSH]^-$, (h) $[CH_3Hg(SH)_2]^-$, (i) **TS5**, and (j) **TS6**. The small red spheres correspond to bond critical points.

Selected parameters of optimized geometrical structures and transition states are collected in Table 1. It is noteworthy that the calculated bond lengths of CCM and CH_3HgSH are very close to the experimental values, with the maximum deviation from the experimental data being less than 0.06 Å for the Hg−Cl bond. The molecular structure of the stable $[CH_3HgClSH_2]$

TABLE 1: Interatomic Distances (Å) and Values of Electron Density (eÅ^{-3}) at Bond Critical Points

species	Hg−Cl	Hg−S1	Hg−S2	Hg−C	C−H	S1−H	H−Cl	S2−H	S3−H	N−H	Hg−N
CH_3HgCl	2.340			2.080							
	(2.282[b])			(2.061[b])							
	0.629			*0.854*							
$[CH_3HgCl-SH_2]$	2.356	3.517		2.082							
	0.608	*0.073*		*0.849*							
TS1	2.395	2.519		2.149	2.882	2.182					
	0.566	*0.485*		*0.736*							
TS2	2.391	2.404		2.240	1.963	3.180					
	0.569	*0.604*		*0.597*							
$[CH_3HgCl-SH]^-$	2.732	2.439		2.133							
	0.281	*0.556*		*0.764*							
TS3	2.783	2.589		2.103		1.490	1.804				
	0.260	*0.423*		*0.801*		*1.006*	*0.457*				
CH_3HgSH		2.379		2.097							
		(2.380[c])		(2.090[c])							
		0.637		*0.830*							
$[CH_3HgSH-SH_2]$		2.388	3.542	2.098							
		0.624	*0.070*	*0.828*							
TS4		2.357	2.755	2.387	1.445			1.715			
		0.648	*0.312*	*0.458*	*0.750*			*0.621*			
$[CH_3Hg(SH)_2]^-$		2.562	2.562	2.172							
		0.436	*0.436*	*0.697*							
TS5		2.460	2.455	2.493	1.516				1.629		
		0.529	*0.533*	*0.367*	*0.641*				*0.737*		
TS6		2.495	2.495	2.468	1.420				1.665		
		0.493	*0.493*	*0.367*	*0.785*				*0.679*		
$[CH_3HgSH-NH_4]^{+1}$		2.352		2.118	2.383					1.033	
		0.673		*0.797*	*0.088*					*2.116*	
TS7		2.320		2.295	1.296					1.553	
		0.701		*0.522*	*1.025*					*0.560*	
$[NH_3HgSH-CH_4]^{+1}$		2.307			2.452					1.022	2.183
		0.723			*0.065*					*2.192*	*0.623*
$[Hg(SH)_2-CH_4-N\,H_3]$		2.355	2.355	4.925	1.091					2.644	
		0.659	*0.659*		*1.823*					*0.059*	
$[CH_3HgSH-H_2S-NH_3]$		2.404	3.438	2.097		2.699				1.019	
		0.604	*0.087*	*0.828*		*0.074*				*2.209*	
$[Hg(CH_3)_2SH]^-$		2.837		2.152							
		0.264		*0.743*							
TS8		2.868		2.370	1.421	1.745					
		0.258		*0.467*	*0.800*	*0.584*					
TS9		2.486	3.491	2.525	1.627			1.555			
		0.506		*0.349*	*0.506*			*0.863*			

[a] Electron density (eÅ^{-3}) at bond critical point in italics. [b] Experimental bond distances: Gordy, W.; Sheridan, J. *J. Chem. Phys.* **1954**, *22*, 92. [c] Experimental bond distances: Holloway, C. E.; Melnik, M. *J. Organomet. Chem.* **1995**, *495*, 1.

complex is displayed in Figure 1a. The small red spheres in Figures 1−4 correspond to bond critical points (BCPs), whose properties provide information about the nature of the bonding. The value of the electron density $\rho(r_c)$ at the BCP depends on the interatomic distance and degree of coordination of the atoms and is often used as a measure of bond strength for similar types of bonds.[26,37] The Hg−S distance of $[CH_3HgClSH_2]$ is 3.517 Å, and the Cl−Hg−C bond angle is 177.3°. The value of $\rho(r_c)$ at the Hg−S BCP is 0.073 eÅ^{-3}. It is clear that the Hg−SH_2 bond is weak.

In searching for possible mechanisms for the protonolysis of CMM by the thiol group of cysteine, we studied intramolecular proton transfer from the complexed H_2S to the CH_3 group. The overall reaction is summarized by

$$CH_3HgCl + H_2S \rightarrow [CH_3HgClSH_2] \rightarrow \mathbf{TS1} \rightarrow [CH_3HgHClSH] \rightarrow \mathbf{TS2} \rightarrow ClHgSH + CH_4 \quad (1)$$

In this case, protonolysis of the Hg−C bond occurs in a stepwise fashion. Starting from $[CH_3HgClSH_2]$, we found two transition states, TS1 and **TS2**, and the intermediate $[CH_3HgHClSH]$. The molecular structures of **TS1** and **TS2** are displayed in Figure 1b and c, respectively. It is interesting to note that there are no bond paths between S1 and H of **TS1** and C and H of **TS2**. Nevertheless, we expect that the delocalization indexes are undoubtedly >0.1 between these pairs of atoms.[38] Energies are collected in Table 2. Such a frontside transfer of the proton effectively leads to retention of the configuration at the methyl group and would be consistent with observations by Begley et al.[18] on more complex alkylmercurials. The imaginary frequency of **TS1** corresponds to the mode for proton transfer from H_2S to the Hg atom, leading to formation of the four-coordinate species $[CH_3HgHClSH]$, which is 5.2 kcal mol^{-1} lower in energy than **TS1**. The imaginary frequency of **TS2** corresponds to a proton transfer from the Hg atom to the CH_3 group, leading to cleavage of the Hg−C bond. However, the barriers are very high; for the first step involving **TS1** the barrier is 59.2 kcal mol^{-1} at the B3PW91/ECP60MWB level. With a relativistic correction at the DKH level, the barrier decreases to 50.6 kcal mol^{-1} (Table 2, column 3). We also performed single-point calculations on the reactants and transition structures of reaction 1 in the water solvent field using the PCM method[39,40] to establish whether a polar effect (of the solvent) alters the barriers without inclusion of explicit solvation. The data are collected in column 4 of Table 2. Whereas the energies of $[CH_3HgClSH_2]$ and **TS1** are lowered significantly, the barrier decreased only

TABLE 2: Energies of Substrates and Transition States at the MWB and DKH Levels and in the Water Solvent Field

species	E_0 (MWB + ZPE)	E_{elec} (DKH)	$E_{elec(sf)}$ (PCM)
H_2S	−399.346 006	−400.331 929	
CH_3HgCl	−653.656 250	−20 085.673 407	
$[CH_3HgCl-SH_2]$	−1053.004 789	−20 486.012 943	−1053.067 894
TS1	−1052.910 439	−20 485.932 218	−1052.996 464
TS2	−1052.914 845	−20 485.938 075	−1052.997 810
$[CH_3HgCl-SH]^-$	−1052.501 148	−20 485.503 181	
TS3	−1052.981 726	−20 485.988 085	−1053.045 885
HCl	−460.765 198	−462.030 991	
CH_3HgSH	−592.225 895	−20 023.962 120	
$[CH_3HgSH-SH_2]$	−991.573 897	−20 424.300 878	−991.642 206
TS4	−991.511 494	−20 424.236 711	−991.576 896
$[CH_3Hg(SH)_2]^-$	−991.059 588	−20 423.779 778	
$[CH_3Hg(SH)_2-H_2S]^-$	−1390.416 574	−20 824.126 724	−1390.552 902
TS5	−1390.381 792	−20 824.089 775	−1390.513 096
$[H_2S-CH_3Hg(SH)_2]^-$	−1390.409 619	−20 824.118 921	
TS6	−1390.387 846	−20 824.092 611	
$[CH_3HgSH-NH_4]^+$	−649.070 450	−20 080.890 359	−649.288 303
TS7	−649.043 056	−20 080.857 654	−649.230 274
$[NH_3HgSH-CH_4]^+$	−649.095 933	−20 080.908 607	
$[Hg(CH_3)_2SH]^-$	−632.119 676	−20 063.916 317	
$[Hg(CH_3)_2-SH_2]$	−632.650 823	−20 064.453 386	
TS8	−632.599 295	−20 064.400 525	
$[Hg(CH_3)_2SHSH_2]^-$	−1031.482 873	−20 464.268 830	
TS9	−1031.450 305	−20 464.232 969	

TABLE 3: QTAIM Charges (e) and Barriers (ΔE_{elec}, kcal mol^{-1}) of Protonolysis at the DKH Level

	QTAIM charges		
species	C	CH_3	ΔE_{elec}
$[CH_3HgCl-SH_2]$	−0.287	−0.096	50.6
$[CH_3HgSH-SH_2]$	−0.307	−0.148	36.0
$[CH_3Hg(SH)_2-SH_2]^-$	−0.311	−0.263	23.2
$[H_2S-CH_3Hg(SH)_2]^-$	−0.335	−0.321	16.5
$[CH_3HgSH-NH_4]^+$	−0.369	−0.167	20.5
$[Hg(CH_3)_2-SH_2]$	−0.350	−0.254	33.2
$[Hg(CH_3)_2SH-SH_2]^-$	−0.333	−0.306	22.5

slightly to 44.8 kcal mol^{-1}. In our view, the high barriers for reaction 1 preclude it as a biologically important process. Nevertheless, we tested the validity of using H_2S in reaction 1, choosing the less computationally demanding CH_3SH instead of cysteine. With CH_3SH, the barrier decreased marginally to 58.2 kcal mol^{-1} at the B3PW91/ECP60MWB level relative to 59.2 kcal mol^{-1} obtained with H_2S. As expected from the small difference in the barriers, the geometries of the transition states at Hg were similar (Cartesian coordinates and E_0 values are included in the Supporting Information).

We also searched for a transition state for a single-step intramolecular transfer of a proton from H_2S to Cl in the complex $[CH_3HgClH_2S]$ and located **TS3**, whose molecular structure is displayed in Figure 1d. Its imaginary frequency corresponds to the transfer of H from H_2S to Cl.

$$CH_3HgCl + H_2S \rightarrow [CH_3HgClH_2S] \rightarrow \mathbf{TS3} \rightarrow CH_3HgSH + HCl \quad (2)$$

The barrier at the B3PW91/ECP60MWB level was found to be 12.9 kcal mol^{-1}. It is seen that both the Hg−Cl and Hg−S bonds are lengthened relative to the bonds in CH_3HgCl and $[CH_3HgClSH]^-$. To confirm that **TS3** connects reactants and products in reaction 2, we performed an intrinsic reaction coordinate (IRC)[41,42] calculation and optimized the structures obtained at the two minima. In proceeding forward from **TS3**, products CH_3HgSH and HCl are observed, whereas in going in the reverse direction, the reactants CH_3HgCl and H_2S are formed. Therefore, according to reactions 1 and 2, the first bond to break in CMM coordinated with one thiol group should be Hg−Cl rather than Hg−C. Water solvent-field calculations on $[CH_3HgClH_2S]$ and **TS3** yielded a marginally higher barrier (13.8 kcal mol^{-1}). This result suggests a possible low-energy pathway for the conversion of CMM into $CH_3-Hg-SR$ species under biotic conditions. We evaluated the impact of replacing H_2S with CH_3SH in reaction 2 and found that the effect was smaller than in the case of reaction 1. At the B3PW91/ECP60MWB level, the barrier for the reaction with CH_3SH was 12.7 kcal mol^{-1}, whereas with H_2S, it was 12.9 kcal mol^{-1}. As expected from the small difference in the barriers, the geometries of the transition states at Hg are similar (Cartesian coordinates and E_0 values are included in the Supporting Information). The results with CH_3SH and H_2S for reactions 1 and 2 validate the use of H_2S in our computational study.

Previous models[19,20] and chemistry[43] suggested that the degradation of organomercurials could involve more than one thiol/thiolate group. Consequently, we considered the possibility that protonation by −SH of a second cysteine residue group could lead to demethylation of CH_3HgSH. One of the simplest reactions would involve a backside attack of CH_3 by H_2S to cleave the Hg−C bond with inversion. However, we were unable to find a transition state for backside protonation by H_2S. Consequently, we carried out a scan calculation to probe the potential energy surface by varying the Hg−C and H−SH interatomic distances. Although backside proton transfer from H_2S to CH_3 was achieved, the barrier for this reaction was greater than 59.0 kcal mol^{-1}, yielding $HgSH^+$, CH_4, and SH^- as products. This is the case because the two oppositely charged ions $HgSH^+$ and SH^- are screened by the neutral product CH_4. Nevertheless, we examined the complexation of H_2S with CH_3HgSH and found the stable complex $[CH_3HgSH-H_2S]$, whose molecular structure is displayed in Figure 1e. As was the case for CMM, H_2S binds weakly to CH_3HgSH; the Hg−H_2S distance is 3.542 Å, and $\rho(r_c)$ at the BCP has a value of 0.070 eÅ^{-3}. Using $[CH_3HgSH-H_2S]$ as a starting point, we located transition state **TS4** (its molecular structure is displayed in Figure 1f) for proton transfer from H_2S to CH_3.

$$CH_3HgSH + H_2S \rightarrow [CH_3HgSH\text{-}H_2S] \rightarrow \mathbf{TS4} \rightarrow Hg(SH)_2 + CH_4 \quad (3)$$

The imaginary frequency of TS4 corresponds to the mode for proton transfer. IRC calculations in the forward and reverse directions from **TS4** yielded the products and reactants as shown in reaction 3. The barrier at the B3PW91/ECP60MWB level is high at 39.2 kcal mol^{-1}. At the relativistic DKH level, the barrier for reaction 3 is lowered slightly to 36.0 kcal mol^{-1} (see Table 2, column 3). A similar barrier was found for the protonation of methylmercury methanethiolate by methanethiol (39.0 kcal mol^{-1}) at the MP2 level.[21] We also calculated the barrier by embedding $[CH_3HgSH-H_2S]$ and **TS4** in the water solvent field. However, the barrier remained high at 40.9 kcal mol^{-1}. Consequently, reaction 3 is not a biologically relevant process. According to Wilhelm et al.,[21] one of the main factors that determines the barrier in the protonolysis reaction is the mercury coordination. The barrier in reaction 3 is smaller than the barrier in reaction 1 by ~20 kcal mol^{-1}. Because the mercury coordination environments of $[CH_3HgCl-SH_2]$ and $[CH_3HgSH-SH_2]$ are the same, other factors must come into play. The dependence of Hg−C bond lengths on the charges on ligand atoms has been reported[23,24] for MeHgX compounds with X = Cl, Br, I, PH_3, and $(PH_3)_3$. It was found that the cleavage of Hg−C bond was enhanced as the negative charge on the CH_3 group increased and the electronegativity of the ligand groups decreased in the order PH_3 > Cl > Br > I > $(PH_3)_3$.[23,24] Consequently, we calculated the AIM charges on the carbon atom and methyl group of the reactants (see Table 3). Higher negative charges are seen on the carbon atom and methyl group of $CH_3HgSH-SH_2$ for reaction 3 than on those of $CH_3HgCl-SH_2$ for reaction 1. Thus, similarly to Barone et al., we observed a decrease of the energy barrier for protonolysis with increasing negative charge on the methyl group.

We explored the coordination of CMM and DMM with HS^- because HS^- ($pK_1 = 7.02$) and Cys-S^- ($pK_1 = 8.40$)[44,45] are common in aqueous solution. As expected, HS^- binds strongly with CMM, yielding $[CH_3HgClSH]^-$, whose molecular structure is displayed in Figure 1g. The Hg−S distance is 2.439 Å, and the value of $\rho(r_c)$ at Hg−S BCP is 0.556 $eÅ^{-3}$. Contrary to the expectation of Moore et al.,[19] the binding of one HS^- moiety to CCM does not weaken/activate the Hg−C bond. Although Hg is tricoordinate, the Hg−C bond distance (2.133 Å) is only 0.053 Å longer than it was in CMM. On the other hand, the Hg−Cl bond lengthened to 2.732 from 2.340 Å, and the value of $\rho(r_c)$ at the Hg−Cl BCP decreased dramatically to 0.281 from 0.629 $eÅ^{-3}$. That the Hg−Cl bond was weakened suggests that it is this bond that should be preferentially protonolyzed by a thiol group of cysteine (or the −OH group of tyrosine). This result suggests a low-energy pathway for the conversion of CMM into $CH_3-Hg-SR$ species under biotic conditions (see reaction 2). SH^- also binds strongly to CH_3HgSH (reaction 4); formation of $[CH_3Hg(SH)_2]^-$ is a highly exothermic process, occurring without a barrier.

$$CH_3HgSH + SH^- \rightarrow [CH_3Hg(SH)_2]^- \quad (4)$$

The molecular structure of $[CH_3Hg(SH)_2]^-$ is displayed in Figure 1h. The Hg−S1 and Hg−S2 bonds exhibited identical internuclear distances (2.562 Å) and values of $\rho(r_c)$ (0.436 $eÅ^{-3}$) at the BCPs. Our computational results compare favorably with the Hg−S bond lengths (2.40−2.51 Å) reported for the $[Hg(SR)_3]^-$ moiety in MerB as determined experimentally by EXAFS spectroscopy.[46,47] Interestingly, the Hg−C bond length of $[CH_3Hg(SH)_2]^-$ did not change significantly relative to the CH_3-Hg bonds of CH_3HgCl and CH_3HgSH.

With the expectation that cleavage of the Hg−C bond of negatively charged $[CH_3Hg(SH)_2]^-$ would occur more easily than in the case of the neutral species CH_3HgCl and CH_3HgSH, we studied the protonolysis of $[CH_3Hg(SH)_2]^-$ by H_2S (reaction 5) to model its reaction with R−SH of cysteine.

$$[CH_3Hg(SH)_2]^- + SH_2 \rightarrow [CH_3Hg(SH)_2\text{-}H_2S]^- \rightarrow \mathbf{TS5} \rightarrow [Hg(SH)_3]^- + CH_4 \quad (5)$$

We located transition state TS5 (Figure 1i), and its imaginary frequency corresponds to the mode for proton transfer from H_2S to CH_3 that results in the cleavage of the Hg−C bond. The barrier for this reaction is 21.8 kcal mol^{-1} at the B3PW91/ECP60MWB level. The relativistically corrected barrier at the DKH level is 23.2 kcal mol^{-1} (Table 2, column 3), and in the water solvent field, the barrier is 24.9 kcal mol^{-1}. The molecular structure of **TS5** is displayed in Figure 1i. The Hg−C bond distance in **TS5** increases from 2.172 Å in $[CH_3Hg(SH)_2]^-$ to 2.493 Å, and the value of $\rho(r_c)$ decreases from 0.697 to 0.367 $eÅ^{-3}$. An IRC calculation from **TS5** in the forward and reverse directions yielded the products and reactants of reaction 5. From Table 3, it is seen that the negative charges on the carbon atom and methyl group of $[CH_3Hg(SH)_2-SH_2]^-$ are higher than the charges for $[CH_3HgSH-SH_2]$ in reaction 3 and $[CH_3HgCl-SH_2]$ in reaction 1. The barrier for reaction 5 is considerably lower than the barriers of reactions 1 and 3. A decreased barrier for protonolysis correlates with a higher negative charge on the methyl group and coordination of the mercury.

We also explored the protonolysis of $[CH_3Hg(SH)_2]^-$ with inversion of configuration at the CH_3 via backside approach of H_2S. The complex $[H_2S-CH_3Hg(SH)_2]^-$, in which H_2S is connected to the C atom through a hydrogen bond, was located first. Complex $[H_2S-CH_3Hg(SH)_2]^-$ decomposed via transition state **TS6** (molecular structure displayed in Figure 1j) to the products shown in reaction 6.

$$[CH_3Hg(SH)_2]^- + H_2S \rightarrow [H_2S-CH_3Hg(SH)_2]^- \rightarrow \mathbf{TS6} \rightarrow Hg(SH)_2 + CH_4 + SH^- \quad (6)$$

Its imaginary frequency corresponds to the mode for proton transfer from H_2S to CH_3. In this case, the barrier is 13.7 kcal mol^{-1}. Interestingly, the products—$Hg(SH)_2$, CH_4, and SH^-—derived from an IRC calculation and optimization were less stable than products $[Hg(SH)_3]^-$ and CH_4 of reaction 5 by 38.7 kcal mol^{-1}. This is not surprising because CH_4 screens SH^- from $Hg(SH)_2$ and precludes the formation of the stable complex $[Hg(SH)_3]^-$.

From the point of view of a reaction within MerB, however, the enzyme must divest itself of the products, for which reaction 6 would appear ideal, as external thiolate (required for enzyme turnover[19] or for transfer to MerA[48]) could rapidly ligand exchange with a dicoordinate $Cys^{96}-Hg-Cys^{159}$. In addition, Benison et al.[48] have shown that a tricoordinate Hg complex of enzyme, $[Cys^{96}-Hg-dithiothreitol]^-$, is very difficult to exchange with external cysteinate. However, for other aryl or alkyl mercurials, it is clear from stereochemical evidence[18,19] that protonolysis takes place with retention of configuration and must therefore proceed through a frontside approach of the proton following reaction 5. Our computations do not per se differentiate between frontside and backside protonolysis within MerB, but they do strongly suggest that protonolysis should take place on a tricoordinate Hg(II) intermediate as opposed to a dicoordinate species as proposed by Benison et al.[48] Consequently, the sequence of reactions 2, 4, and 5 or 6, which includes the binding of SH^- followed by protonation, appears to define a plausible model for demethylation of CH_3HgCl via binding with

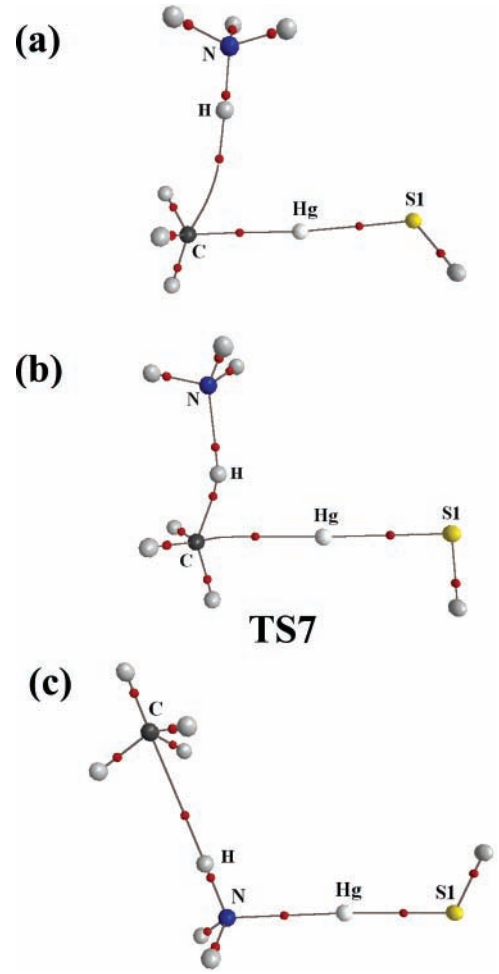

Figure 2. Calculated molecular structures of (a) $[CH_3HgSH-NH_4]^+$, (b) **TS7**, and (c) $[CH_3HgSH-NH_4]^+$. The small red spheres correspond to bond critical points.

cysteine and cysteine thiolate and lends support for the proposals by Moore et al.,[19] Pitts and Summers,[20] and Di Lello et al.[22]

Lysine and other ammonium residues are common in proteins. Therefore, we next turned our attention to protonolysis reactions involving ammonium acids, which we simulated as NH_4^+. The use of NH_4^+ as a model for lysine$-NH_3^+$ is valid because their pK_a values differ by only 1.5 pH units in H_2O. NH_4^+ forms a complex with the methyl group of CH_3HgSH through a hydrogen bond. The molecular structure of the complex is displayed in Figure 2a. We used this complex as a starting point and located transition state **TS7** (Figure 2b) for protonolysis of the Hg−C bond of CH_3HgSH via frontside approach (reaction 7).

$$CH_3HgSH + NH_4^+ \rightarrow [CH_3HgSH-NH_4]^+ \rightarrow \mathbf{TS7} \rightarrow [HgSHNH_3]^+ + CH_4 \quad (7)$$

At the B3PW91/ECP60MWB level, the barrier is 17.2 kcal mol^{-1}. The relativistically corrected value is 20.5 kcal mol^{-1} at the DKH level (Table 2, column 3). The imaginary frequency corresponds to the mode for movement of a proton from NH_4^+ toward the methyl group. It is seen that the negative charge (−0.369) on the carbon of $[CH_3HgSH-NH_4]^+$ is higher than values for the complexes of reactions 1, 3, and 5 (see Table 3), even though $[CH_3HgSH-NH_4]^+$ bears a net positive charge. The methyl group of $[CH_3HgSH-NH_4]^+$ bears a charge of −0.167, which is lower than the value for $[CH_3Hg(SH)_2-H_2S]^-$ of reaction 5 but higher than the value for $[CH_3HgSH-H_2S]$ of reaction 3. Thus, regardless of the net charge of the complex, the barrier for protonolysis decreases as the negative charge on the carbon atom and methyl group increases. An IRC calculation in the forward direction followed by a geometry optimization of the minimum-energy structure yields $[CH_3HgNH_3]^+$ hydrogen bonded with CH_4 as the products of reaction 7. The molecular structure of $[NH_3HgSH-CH_4]^+$ is displayed in Figure 2c. In the water solvent field, the barrier increases to 36.4 kcal mol^{-1}. The increase (+19.2 kcal mol^{-1}) arises from the fact that the polar stabilization of the reactant, $[CH_3HgSH-NH_4]^+$, is higher than that of **TS7**; the electrostatic solute−solvent contribution to E_{elec} for $[CH_3HgSH-NH_4]^+$ is −76.4 kcal mol^{-1}, whereas for **TS7**, it is −61.4 kcal mol^{-1}. We were unable to locate a transition state for backside protonolysis of CH_3HgSH by NH_4^+. Perhaps the products lie too high on a potential energy surface with respect to reactants, as CH_4, located between $HgSH^+$ and NH_3, would effectively screen and prevent them from coordination.

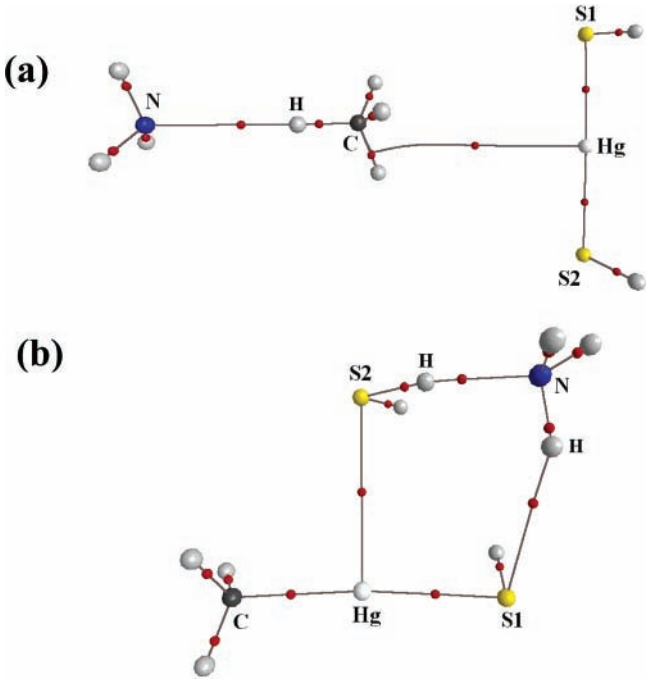

Figure 3. Calculated molecular structures of (a) $[NH_3HgSH-CH_4]^+$ and (b) $[CH_3HgSH-H_2S-NH_3]$. The small red spheres correspond to bond critical points.

Next, we examined the reaction between $[CH_3Hg(SH)_2]^-$ and NH_4^+ by first attempting to locate a complex that would lead to protonolysis by inversion with NH_4^+ oriented toward the backside of $[CH_3Hg(SH)_2]^-$. No stable complex between $[CH_3Hg(SH)_2]^-$ and NH_4^+ was observed. With the distance between the hydrogen of NH_4^+ and the carbon of the CH_3 of the starting configuration set at 3.0 Å, optimization yielded the neutral species $Hg(SH)_2$, CH_4, and NH_3. The molecular structure of the minimum-energy complex of these products is displayed in Figure 3a. Amazingly, protonolysis with inversion occurred without a barrier. On the other hand, in optimizing $[CH_3Hg(SH)_2]^-$ with NH_4^+ in a frontside position [by analogy with **TS5** (Figure 1i)], NH_4^+ simply protonated one SH^- group rather than CH_3, yielding a different set of products: CH_3HgSH, H_2S, and NH_3. The molecular structure of this complex, $[CH_3HgSH-H_2S-NH_3]$, stabilized by hydrogen bonds, is displayed in Figure 3b. This reaction also exhibits no barrier. Overall, judging from our studies with NH_4^+, ammonium species might

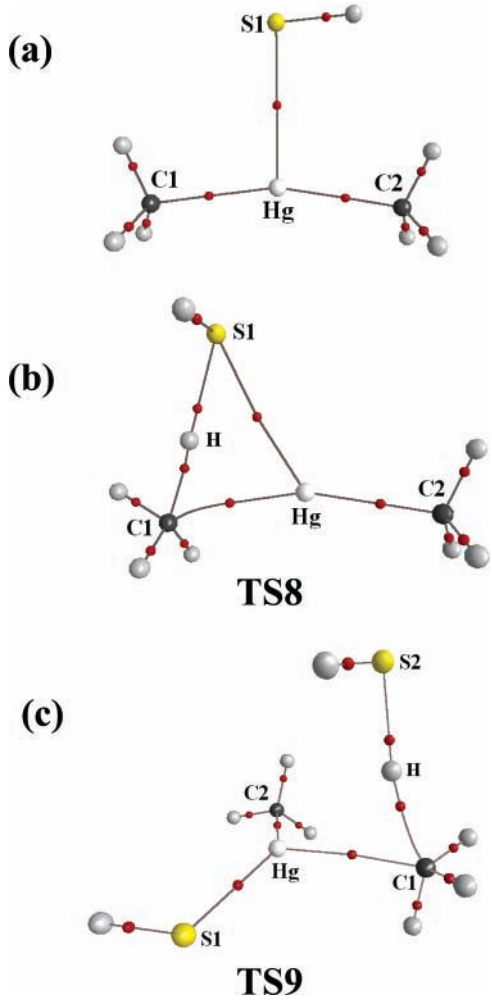

Figure 4. Calculated molecular structures of (a) **TS8**, (b) $[CH_3Hg(SH)_2]^-$, and (c) **TS9**. The small red spheres correspond to bond critical points.

play an important role in the protonolysis of the Hg−C bond, although the solution environment might lessen its catalytic effect.

We compared the protonolysis of dimethylmercury by cysteine to the protonolysis of chloromethylmercury. Barone et al.[24] investigated the protonation of dimethylmercury and methylmercury halides by halogenic acids. They reported that the energy barrier decreased from 34.9 to 20.7 kcal mol^{-1} going from chloromethylmercury to dimethylmercury because of different ligand electronegativity. We searched for the transition state in the protonation of dimethylmercury, $Hg(CH_3)_2$, by H_2S as shown in reaction 8.

$$Hg(CH_3)_2 + H_2S \rightarrow [Hg(CH_3)_2SH_2] \rightarrow \textbf{TS8} \rightarrow CH_3HgSH + CH_4 \quad (8)$$

and located **TS8** (Figure 4b). The barrier for reaction of $[Hg(CH_3)_2SH_2]$ was found to be 33.7 kcal mol^{-1}. Similar to Barone et al.'s observations, the barrier for protonation of dimethylmercury in reaction 8 is substantially lower than that for chloromethylmercury in reaction 1 (59.2 kcal mol). Because this barrier is still substantial, and we noted from reaction 5 that a negative charge on the complex facilitates the demethylation reaction, we decided to explore coordination of dimethylmercury with SH^- and then try to protonate it with H_2S. Indeed, the formation of the complex $[Hg(CH_3)_2SH]^-$ occurs without any barrier.

$$Hg(CH_3)_2 + SH^- \rightarrow [Hg(CH_3)_2SH]^- \quad (9)$$

The molecular structure of $[Hg(CH_3)_2SH]^-$ is displayed in Figure 4a. After obtaining the complex $[Hg(CH_3)_2SH]^-$, we searched for its protonation by H_2S. We found an intermediate and transition state **TS9** (Figure 4c) for the reaction in which frontside protonolysis takes place.

$$[Hg(CH_3)_2SH]^- + H_2S \rightarrow [Hg(CH_3)_2SHSH_2]^- \rightarrow \textbf{TS9} \rightarrow [CH_3Hg(SH)_2]^- + CH_4 \quad (10)$$

The barrier for the second step involving **TS9** is only 20.4 kcal mol^{-1} at the B3PW91/ECP60MWB level. Thus, protonation of $[Hg(CH_3)_2SHSH_2]^-$ by H_2S is similar to reaction 5 with respect to the barrier and the nature of the transition state.

Conclusions

DFT calculations at the B3PW91/ECP60MWB level, including relativistic corrections, provide support for the mechanistic proposals[19,20,22] for the action of MerB in deactivating organomercurials. This result suggests that this level of theory is suitable for studying the bioorganic chemistry of organomercury compounds. Chloromethylmercury demethylation mechanisms were examined by locating transition states and determining barriers for possible sequences of reactions. We predict from these calculations that demethylation of CH_3−Hg is preceded by protonolysis of the Hg−Cl bond, highly activated by complexation with thiol. We found that the intramolecular process has a surprisingly low barrier. Loss of HCl is followed by subsequent complexation with up to two thiolate groups and protonolysis of the Hg−C bond by thiol. The magnitude of the barrier depends on the number of coordinating thiolates: as the number of coordinating thiolates increases, the negative charge on the carbon of the CH_3 group increases and facilitates the protonation reaction. Water solvent-field calculations yielded results that were comparable to our findings for the gaseous phase. Backside protonation the CH_3 group yields the lowest-energy protonolysis route and, from the viewpoint of an enzyme, would be an ideal process to facilitate removal of Hg(II) from the active site. Amino protein residues might also serve as acids. In the gas phase, backside protonolysis of the Hg−C bond of $[CH_3Hg(SH)_2]^-$ by the ammonium ion (NH_4^+) occurs without a detectable barrier.

Acknowledgment. We gratefully acknowledge financial support from the Natural Science and Engineering Research Council of Canada and SHARCNET [Shared Hierarchical Academic Research Computing Network (of Ontario)] for providing computing resources at McMaster University and a Postdoctoral Fellowship for B.N.

Supporting Information Available: Cartesian coordinates of optimized geometries and transition states. This material is available free of charge via the Internet at http://pubs.acs.org.

References and Notes

(1) Wood, J. M. In *Advances in Environmental Science and Technology*; Pitts, J. N., Metkalf, R. L., Eds.; Wiley: New York 1971; Vol. 2, p 39.

(2) Morel, F. M. M.; Kraepel, A. M. L.; Amyot, M. *Annu. Rev. Ecol. Syst.* **1998**, *29*, 543.

(3) Goyer, R. A. *Toxicological Effects of Methylmercury*; National Academy Press: Washington, DC, 2000.

(4) Harris, H. H.; Pickering I. J.; Graham, N. G. *Science* **2003**, *301*, 1203.

(5) Bloom, N. S.; Watras, C. J.; Hurley, J. P. *Water Air Soil Pollut.* **1991**, *56*, 477.
(6) Boudou, A.; Ribeyre, F. *Metal Ions Biol. Syst.* **1997**, *34*, 289.
(7) Marvin-Dipasquale, M. C.; Oremland, R. S. *Environ. Sci. Technol.* **1998**, *32*, 2556.
(8) Marvin-Dipasquale, M. C.; Agee, J.; Oremland, R. S.; Thomas, M.; Krabbenhoft, D.; Gilmour, C. C. *Environ. Sci. Technol.* **2000**, *34*, 4908.
(9) Robinson, J. B.; Tuovinen, O. H. *Microbiol. Rev.* **1984**, *48*, 95.
(10) Amyot, M.; Mierle, G.; Lean, D.; McQueen, D. *Geochim. Cosmochim. Acta* **1997**, *61*, 975.
(11) Sellers, P.; Kelly, S. A.; Rudd, J. W. M.; Mac-Hutchon, A. R. *Nature* **1996**, *380*, 694.
(12) Suda, I.; Suda, M.; Hirayama, K. *Arch. Toxicol.* **1993**, *67*, 365.
(13) Inoko, M. *Environ. Pollut. B* **1981**, *2*, 3.
(14) Tossell, J. A. *J. Phys. Chem. A* **1998**, *102*, 3587.
(15) Chen. J.; Pehkonen, S. O.; Lin, C. J. *Water Res.* **2003**, *37*, 2496.
(16) Brown, N. L.; Ford S. J.; Pridmore, R. D.; Fritzinger, D. C. *Biochemistry* **1983**, *22*, 4089.
(17) Misra, T. K.; Brown, N. L.; Fritzinger, D. C.; Pridmore, R. D.; Barnes W. M.; Haberstroh, L.; Silver, S. *Proc. Natl. Acad. Sci. U.S.A.* **1984**, *81*, 5975.
(18) Begley, T. P.; Walts, A. E.; Walsh, C. T. *Biochemistry* **1986**, *25*, 7192.
(19) Moore, M. J.; Distefano, M. D.; Zydowsky, L. D.; Cummings, R. T.; Walsh, C. T. *Acc. Chem. Res.* **1990**, *23*, 301.
(20) Pitts, K. E.; Summers, A. O. *Biochemistry* **2002**, *41*, 10287.
(21) Wilhelm, M.; Deekin, S.; Berssen, E.; Saak, W.; Lutzen, A.; Koch, R.; Strasdeit, H. *Eur. J. Inorg. Chem.* **2004**, 2301.
(22) Di Lello, P.; Benison, G. C.; Valafar, H.; Pitts, K. E.; Summers, A. O.; Legault, P.; Omichinski, J. G. *Biochemistry* **2004**, *43*, 8322.
(23) Barone, V.; Bencini, A.; Totti, F.; Uytterhoeven, M. G. *J. Phys. Chem.* **1995**, *99*, 12743.
(24) Barone, V.; Bencini, A.; Totti, F.; Uytterhoeven, M. G. *Organometallics* **1996**, *15*, 1465.
(25) Barone, V.; Bencini, A.; Totti, F.; Uytterhoeven, M. G. *Int. J. Quantum Chem.* **1997**, *61*, 361.
(26) Bader, R. F. W. *Atoms in Molecules*; Oxford Science Publications: Oxford, U.K., 1990.
(27) Biegler-Konig, F. *AIM 2000*; University of Applied Science: Bielefeld, Germany, 1998−2000.
(28) Yoon, S. J.; Diener, L. M.; Bloom, P. R.; Nater, E. A.; Bleam, W. F. *Geochim. Cosmochim. Acta* **2005**, *69*, 1111.
(29) Frisch, M. J.; Trucks, G. W.; Schlegel, H. B.; Scuseria, G. E.; Robb, M. A.; Cheeseman, J. R.; Zakrzewski, V. G.; Montgomery, J. A., Jr.; Stratmann, R. E.; Burant, J. C.; Dapprich, S.; Millam, J. M.; Daniels, A. D.; Kudin, K. N.; Strain, M. C.; Farkas, O.; Tomasi, J.; Barone, V.; Cossi, M.; Cammi, R.; Mennucci, B.; Pomelli, C.; Adamo, C.; Clifford, S.; Ochterski, J.; Petersson, G. A.; Ayala, P. Y.; Cui, Q.; Morokuma, K.; Malick, D. K.; Rabuck, A. D.; Raghavachari, K.; Foresman, J. B.; Cioslowski, J.; Ortiz, J. V.; Stefanov, B. B.; Liu, G.; Liashenko, A.; Piskorz, P.; Komaromi, I.; Gomperts, R.; Martin, R. L.; Fox, D. J.; Keith, T.; Al-Laham, M. A.; Peng, C. Y.; Nanayakkara, A.; Gonzalez, C.; Challacombe, M.; Gill, P. M. W.; Johnson, B. G.; Chen, W.; Wong, M. W.; Andres, J. L.; Head-Gordon, M.; Replogle, E. S. and Pople, J. A. *Gaussian 98*, revision A.9; Gaussian, Inc.: Pittsburgh, PA, 1998.
(30) Perdew, J. P.; Wang, Y. *Phys. Rev. B* **1992**, *45*, 13244.
(31) Andrae, D.; Haeussermann U.; Dolg, M.; Stoll, H.; Preuss, H. *Theor. Chim. Acta* **1990**, *77*, 123.
(32) Cox, H.; Stace, A. J. *J. Am. Chem. Soc.* **2004**, *126*, 3939.
(33) Gleichmann, M. M.; Heb B. A. *Chem. Phys. Lett.* **1994**, *227*, 229.
(34) Jong, W. A.; Harrison, R. J.; Dixon, D. A. *J. Chem. Phys.* **2001**, *114*, 48.
(35) Casas, J. S.; Jones, M. M. *J. Inorg. Nucl. Chem.* **1980**, *42*, 99.
(36) Smith, R. M.; Martell, A. E. *Critical Stability Constants*; Plenum Press: New York, 1976; Vol. 4: Inorganic Complexes.
(37) Gibbs, G. V.; Boisen, M. B.; Beverly, L. L.; Rosso, K. M. *Rev. Miner. Geochem.* **2002**, *42*, 345.
(38) Wang, Y.-G.; Matta, C.; Werstiuk, N. H. *J. Comput. Chem.* **2003**, *24*, 1720.
(39) Miertus, S.; Tomasi, J. *Chem. Phys.* **1982**, *65*, 239.
(40) Cossi, M.; Barone, V.; Mennucci, B.; Tomasi, J. *Chem. Phys. Lett.* **1996**, *255*, 327.
(41) Gonzalez, C.; Schlegel, H. B. *J. Chem. Phys.* **1989**, *90*, 2154.
(42) Gonzalez, C.; Schlegel, H. B. *J. Phys. Chem.* **1990**, *94*, 5523.
(43) Rabenstein, D. L.; Reid, R. S. *Inorg. Chem.* **1984**, *23*, 1246.
(44) Rueben, D. M. E.; Bruice, T. C. *J. Am. Chem. Soc.* **1976**, *98*, 114.
(45) *NIST Critically Selected Stability Constants of Metal Complexes*; NIST Standard Reference Database; National Institute of Standards and Technology (NIST): Gaithersburg, MD, 2001.
(46) Gruff, E. S.; Koch, S. A. *J. Am. Chem. Soc.* **1990**, *112*, 1245.
(47) Wright, J. G.; Tsang, H. T.; Penner-Hahn, J. E.; O'Halloran, T. V. *J. Am. Chem. Soc.* **1990**, *112*, 2434.
(48) Benison, G. C.; Di Lello, P.; Shokes, J. E.; Cosper, N. J.; Scott, R. A.; Legault, P.; Omichinski, J. G. *Biochemistry* **2004**, *43*, 8333.